A Time-Domain Model for High-Frequency Wheel/Rail Interaction Including Tangential Friction

Astrid Pieringer, Wolfgang Kropp

10ème **C**ongrès **F**rançais d'**A**coustique

Lyon, 12-16 Avril 2010

A Time-Domain Model for High-Frequency Wheel/Rail Interaction Including Tangential Friction

Astrid Pieringer[1], Wolfgang Kropp[2]

Division of Applied Acoustics / CHARMEC, Chalmers University of Technology, Sven Hultins gata 8a, S-41296 Göteborg, Sweden

[1]astrid.pieringer@chalmers.se, [2]wk@ta.chalmers.se

Lateral forces due to frictional instability are seen as the main reason for the occurrence of curve squeal. Predicting squeal requires thus to describe the high-frequency wheel/rail interaction during curving including the coupling between vertical and lateral directions. In this paper, a time domain approach is presented which includes both vertical and lateral forces and takes into account the non-linear processes in the contact zone. Track and wheel are described as linear systems using impulse response functions that can be pre-calculated. The non-linear, non-steady state contact model is based on an influence function method for the elastic half-space. First results from the interaction model including tangential friction are presented in order to demonstrate the functioning of the approach.

1 Introduction

Curve squeal is a highly disturbing tonal sound generated by a railway vehicle negotiating a sharp curve. This type of noise is commonly attributed to self-excited vibrations of the railway wheel, which are either induced by stick/slip behaviour due to lateral creepage of the wheel tyre on the top of the rail or by contact on the wheel flange [1].

Although many curve squeal models have been proposed in the literature, e.g. the models [2–6], curve squeal remains difficult to predict. On the one hand, this can be attributed to the lack of knowledge about important model parameters, such as e.g. realistic friction coefficients. On the other hand, high-frequency wheel/rail interaction during curving is a complex phenomena, which poses a challenge in modelling. As curve squeal is intrinsically transient and non-linear, models aiming to predict squeal amplitudes have to be formulated in the time-domain. Due to the required computational effort of time-domain solutions, it is usually necessary to simplify wheel, rail and contact dynamics, and, by consequence, the models might not include all the important features of the phenomena.

The aim of the work presented in this paper is to contribute to the modelling and understanding of curve squeal by proposing a detailed time-domain model for dynamic wheel/rail interaction that considers the coupling between vertical and tangential directions. The computational effort is reduced by representing vehicle and track by impulse response functions that are calculated in advance. This technique, which has proven efficient for instance in the area of tyre/road noise [7] and in vertical wheel/rail interaction [8], makes it possible to include a non-linear, non-steady state contact model that is solved at each time step in the interaction model.

2 Wheel/rail interaction model

The wheel/rail interaction model is primarily intended for quasi-static curving of the leading inner wheel in a railway bogie. The model relies on the wheel/rail contact position and the angle of attack of the wheelset (i.e. the lateral creepage) as input parameters. These parameters can be pre-calculated with a vehicle dynamics programme.

Figure 1 shows the reference frame for the wheel/rail interaction model. The x-direction (1-direction) is the rolling direction along the rail. The lateral direction is the y-direction (2-direction) pointing away from the wheel flange. The vertical z-coordinate (3-coordinate) is pointing into the rail. This reference frame is moving with the nominal contact point along the rail.

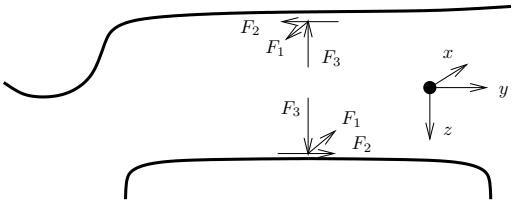

FIG. 1: Reference frame.

2.1 Wheel and track model

The vehicle is represented by a single flexible C20 wheel disregarding the influence of the axle. The wheel is modelled by axi-symmetric finite elements and represented by its modal basis. The receptances of the wheel in the wheel/rail contact point on the wheel tread are calculated by modal superposition.

The track consisting of one continuously supported BV50 rail is modelled with wave-guide finite elements using the the software package WANDS [9]. This model

takes advantage of the two-dimensional geometry of the rail but nonetheless considers the three-dimensional nature of the vibration by assuming a wave-type solution along the rail. Cross-sectional deformations of the rail, which are important for high-frequency applications and lateral dynamics are taken into account.

Figure 2 shows the vertical and lateral point receptances and the vertical/lateral cross receptances of the wheel and the track at the nominal contact point. On the wheel, the nominal contact point is assumed at the centre of the wheel tread. On the rail head, the nominal contact point is assumed at a distance of 1.2 cm from the centre. This offset introduces a coupling between vertical and lateral dynamics of the rail.

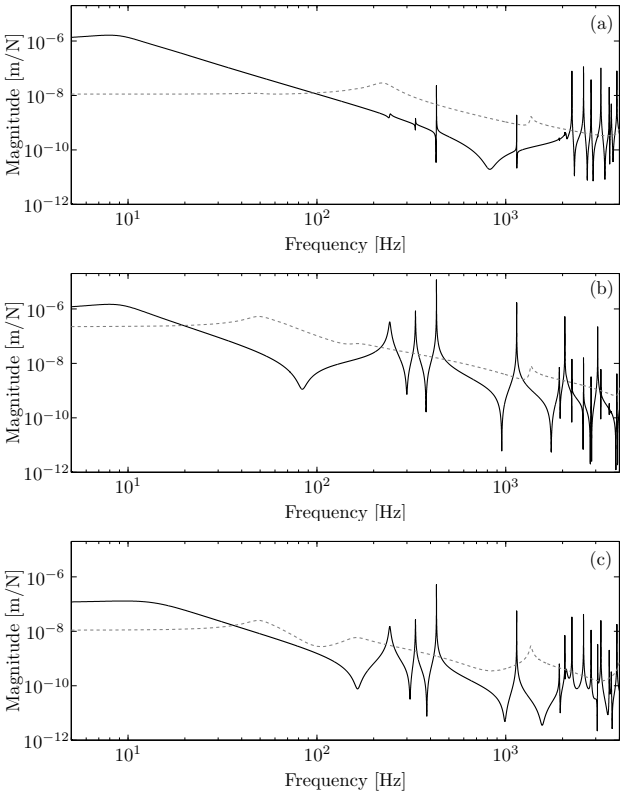

FIG. 2: Magnitudes of the wheel (——) and track receptances (− − −) at contact : (a) vertical point receptance, (b) lateral point receptance, (c) vertical/lateral cross receptance.

The impulse response functions (or Green's functions) of the wheel, g_{ij}^{W}, are obtained by inverse Fourier transform from the wheel receptances, G_{ij}^{W},

$$g_{ij}^{\mathrm{W}}(t) = \mathscr{F}^{-1}\left(G_{ij}^{\mathrm{W}}(f)\right), \qquad i,j = 2,3\,. \tag{1}$$

The subscripts i and j denote the excitation and response direction, respectively. The lateral and vertical displacements of the wheel at the contact point, $\xi_2^{\mathrm{W}}(t)$ and $\xi_3^{\mathrm{W}}(t)$, are then calculated by convoluting the contact forces with the Green's functions

$$\xi_j^{\mathrm{W}}(t) = -\int_0^t \sum_{i=2}^{3} F_i(\tau) g_{ij}^{\mathrm{W}}(t-\tau)\,\mathrm{d}\tau\,, \quad j = 2,3\,. \tag{2}$$

The longitudinal dynamics of the wheel is not taken into account and the influence of wheel rotation is neglected.

The track is represented by a special type of Green's functions denoted moving Green's functions, $g_{ij,v}^{\mathrm{R},x_0}(t)$, which include the motion of the nominal contact point along the rail [10]. The function $g_{ij,v}^{\mathrm{R},x_0}(t)$ describes, for excitation of the rail (index R) in i-direction at the position x_0 at time $t_0 = 0$, the displacement response of the rail in j-direction at a point moving with train speed v away from the excitation, thus at the nominal contact point between wheel and rail. The discrete version of the moving Green's function $g_{ij,v}^{\mathrm{R},x_0}(t)$ is constructed from (ordinary) Green's functions $g_{ij}^{\mathrm{R},\,x_0,\,x_0+\alpha}(t)$, where the superscripts specify the excitation point x_0 and the response point $x_0 + \alpha$ on the rail. The Green's functions $g_{ij}^{\mathrm{R},\,x_0,\,x_0+\alpha}(t)$ are obtained from the corresponding track transfer receptances by inverse Fourier transform

$$g_{ij}^{\mathrm{R},\,x_0,\,x_0+\alpha}(t) = \mathscr{F}^{-1}\left(G_{ij}^{\mathrm{R},\,x_0,\,x_0+\alpha}(f)\right), \quad i,j = 2,3\,. \tag{3}$$

The lateral and vertical displacements of the track at the contact point, $\xi_2^{\mathrm{R}}(t)$ and $\xi_3^{\mathrm{R}}(t)$, are calculated by convoluting the contact forces with the moving Green's functions

$$\xi_j^{\mathrm{R}}(t) = \int_0^t \sum_{i=2}^{3} F_i(\tau) g_{v,ij}^{\mathrm{R},v\tau}(t-\tau)\,\mathrm{d}\tau\,, \quad j = 2,3\,. \tag{4}$$

The longitudinal dynamics of the track is not taken into account.

In the case of the continuously supported track used in this article, the moving Green's functions are independent from the excitation position x_0 on the rail.

2.2 Contact model

The contact model is an implementation of Kalker's model CONTACT [11], which is a three-dimensional, non-steady state rolling contact model based on the assumption that wheel and rail can be locally approximated by elastic half-spaces. In addition to the parameters included in CONTACT, the contact model used in this article considers the combined roughness of wheel and rail on several parallel lines in the rolling direction and the contribution of the structural dynamics of wheel and rail to the creepage.

The potential contact area is divided into N rectangular elements with side lengths Δx and Δy in $x-$ and $y-$direction, respectively. Assuming that wheel and rail are made of the same material, quasi-identity holds and, consequently, normal and tangential contact problem can be solved separately [11].

2.2.1 Normal contact

The normal contact problem consists in determining which elements of the potential contact area are in contact and in calculating the local vertical displacement u_{I3} and the contact pressure p_{I3} in every element I.

The local vertical displacement, which is the displacement difference between rail and wheel

$$u_{I3} = u_{I3}^{\mathrm{R}} - u_{I3}^{\mathrm{W}}\,, \quad I = 1,\ldots,N\,, \tag{5}$$

is related to the contact pressure according to

$$u_{I3} = \sum_{J=1}^{N} A_{I3J3}\, p_{J3}\,, \quad I = 1, \ldots, N\,, \tag{6}$$

where A_{I3J3} are influence coefficients for the elastic half-space. The total vertical contact force, F_3, is obtained by summing the contributions from the different elements

$$F_3 = \sum_{I=1}^{N_e} p_{I3} \Delta x \Delta y\,. \tag{7}$$

Introducing the variable d_I describing the distance between the deformed bodies in each element, the contact conditions are formulated as

$$\begin{aligned} d_I &\geq 0 \\ p_{I3} &\geq 0\ . \\ d_I p_{I3} &= 0 \end{aligned} \tag{8}$$

If contact occurs in a surface element, the distance is zero and the contact pressure is positive. If contact does not occur, the distance is positive and the pressure is zero. Adhesion and penetration are excluded by (8). The distance d_I is obtained as

$$d_I = -\delta + u_{I3} + z_I^{\mathrm{R}} - z_I^{\mathrm{W}} + r_I^{\mathrm{R}} - r_I^{\mathrm{W}}\,, \tag{9}$$

where z_I^{R} and z_I^{W} are the profiles of rail and wheel, r_I^{R} and r_I^{W} are the roughness of rail and wheel and δ is the approach of distant points

$$\delta = \xi_3^{\mathrm{W}} + \xi_3^{\mathrm{S}}(P) - \xi_3^{\mathrm{R}}\,. \tag{10}$$

The variable $\xi_3^{\mathrm{S}}(P)$ is the position of the primary suspension of the wheel corresponding to the nominal preload, P, which represents the vehicle components above the primary suspension.

The normal contact problem is solved with an active set algorithm [11].

2.2.2 Tangential contact model

In frictional rolling contact, the contact area is divided into a stick and a slip area. The tangential contact problem consists in determining which elements are in stick and in slip and in calculating the local tangential displacements $u_{I\tau}$ and tangential stresses $p_{I\tau}$ at the surface.

The relation between local tangential displacements and tangential stresses is given by

$$u_{I\tau} = \sum_{\alpha=1}^{2} \sum_{J=1}^{N} A_{I\tau J\alpha}\, p_{J\alpha}\,, \quad \tau = 1, 2\,, \tag{11}$$

where $A_{I\tau J\alpha}$ are influence coefficients for the elastic half-space. The tangential forces, F_τ, are obtained by summing up the contributions from the different elements

$$F_\tau = \sum_{I=1}^{N} p_{I\tau} \Delta x \Delta y\,, \quad \tau = 1, 2\,. \tag{12}$$

A contact element belongs to the stick area, if the local shift, $S_{I\tau}$, vanishes

$$S_{I\tau} = 0\,, \quad \tau = 1, 2\,. \tag{13}$$

Otherwise the contact element belong to the slip area. The local shift is defined as

$$S_{I\tau} = u_{I\tau} + W_\tau^* - u'_{I\tau}\,, \quad \tau = 1, 2\,. \tag{14}$$

The variable $u'_{I\tau}$ represents the local displacement at the previous time step. In Kalker's formulation, $W_{I\tau}$ is the rigid shift calculated as

$$W_1 = \xi - y\phi \tag{15}$$

$$W_2 = \eta + x\phi\,, \tag{16}$$

where ξ, η and ϕ are the longitudinal, lateral and spin creepage. In this paper, the contribution of the structural dynamics of wheel and track is added to the rigid shift

$$W_1^* = \xi - y\phi \tag{17}$$

$$W_2^* = \eta + x\phi + \left(\xi_2^{\mathrm{R}} - \xi_2^{\mathrm{W}}\right) - \left(\xi_2'^{\mathrm{R}} - \xi_2'^{\mathrm{W}}\right)\,, \tag{18}$$

where $\xi_2'^{\mathrm{R}}$ and $\xi_2'^{\mathrm{W}}$ are the lateral displacements of rail and wheel at the previous time step.

In the slip area, the following relations hold

$$\frac{p_{I\tau}}{\sqrt{p_{I1}^2 + p_{I2}^2}} = -\frac{S_{I\tau}}{\sqrt{S_{I1}^2 + S_{I2}^2}}\,, \quad \tau = 1, 2 \tag{19}$$

$$p_{I1}^2 + p_{I2}^2 = (\mu p_{I3})^2\,, \tag{20}$$

where μ is the friction coefficient, which is assumed constant. Equation (19) assures that the slip occurs in the direction opposite to the tangential stress. Equation (20) states that the tangential stress in the slip zone is equal to the traction bound μp_{I3}.

The tangential contact problem is solved with an active set algorithm [11] combined with the Newton-Raphson method.

3 Simulation results

In this section, first results from the interaction model are presented in order to demonstrate the functioning of the approach. The common model parameters used in the simulations are presented in Table 1. Wheel and rail profiles are assumed cylindrical with wheel radius R_{W} and rail head radius R_{R}. The longitudinal creepage, ξ, and the spin creepage, ϕ, are set to zero in all the simulations presented.

3.1 Comparison to CONTACT

Setting all Green's functions to zero (i.e. assuming quasi-static conditions) and using smooth wheel and rail surfaces makes it possible to verify the interaction model against CONTACT [11, 12].

Figure 3 shows the division of the contact area into stick and slip zones obtained with both models for an imposed lateral creepage of $\eta = 10^{-3}$ and a static preload of $P = F_3 = 65\,\mathrm{kN}$. The results obtained with both models are identical. The rolling direction is the positive x-direction. The slip zone is located at the trailing edge of the contact.

The distribution of total tangential stress corresponding to Figure 3 is presented in Figure 4. The total lateral force is $F_2 = -8.1\,\mathrm{kN}$.

Wheel radius	$R^{\mathrm{W}} = 0.39\,\mathrm{m}$
Rail head radius	$R^{\mathrm{R}} = 0.30\,\mathrm{m}$
Half of wheelset mass	$m_{\mathrm{W}} = 342\,\mathrm{kg}$
Wheel and rail material :	
Young's modulus	$E = 210\,\mathrm{GN/m^2}$
Poisson ratio	$\nu = 0.3$
Density	$\rho = 7860\,\mathrm{kg/m^3}$
Loss factor (rail)	$\eta_{\mathrm{R}} = 0.01$
Material of rail support :	
Young's modulus	$E_E = 4.8\,\mathrm{MN/m^2}$
Poisson ratio	$\nu_{\mathrm{E}} = 0.45$
Density	$\rho_{\mathrm{E}} = 10\,\mathrm{kg/m^3}$
Loss factor	$\eta_{\mathrm{E}} = 0.25$
Train speed	$v = 100\,\mathrm{km/h}$
Static preload	P=65 kN
Primary wheel suspension :	
Stiffness (vertical)	$k_3 = 1.12\,\mathrm{MN/m}$
Damping (vertical)	$c_3 = 13.2\,\mathrm{kNs/m}$
Stiffness (lateral)	$k_2 = 1.12\,\mathrm{MN/m}$
Damping (lateral)	$c_2 = 13.2\,\mathrm{kNs/m}$
Friction coefficient	$\mu = 0.3$
Spatial resolution	$\Delta x = \Delta y = 1\,\mathrm{mm}$

TAB. 1: Model parameters

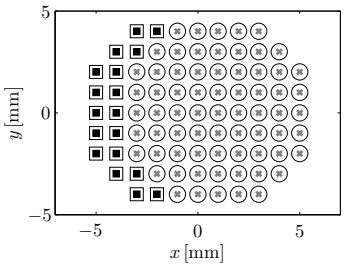

FIG. 3: Division of the contact area : quasi-static case, $\eta = 10^{-3}$. Stick zone : ∘ (CONTACT), x (interaction model) ; Slip zone : □ (CONTACT), □, filled (interaction model).

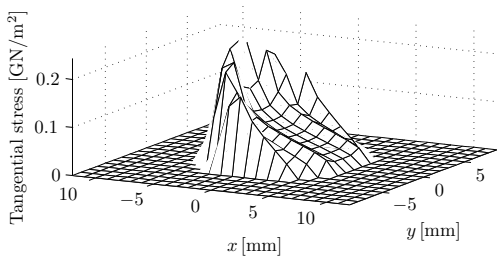

FIG. 4: Distribution of the total tangential stress $\sqrt{p_1^2 + p_2^2}$: quasi-static case, $\eta = 10^{-3}$.

The distribution of lateral stress on line $y = 0$, which is depicted in Figure 5, shows that the result from the interaction model is in excellent agreement with CONTACT. The maximum relative difference between both models does not exceed 0.16% and can be attributed to different round-off practices. This implies that the contact model used in this paper is correctly implemented.

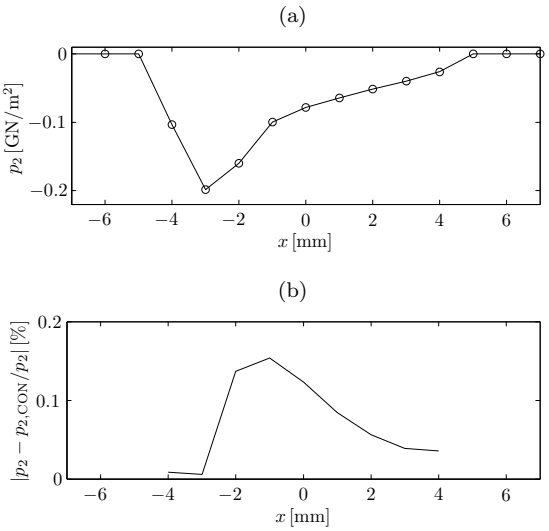

FIG. 5: Lateral tangential stress on line $y = 0$: quasi-static case, $\eta = 10^{-3}$. (a) Amplitude : —— interaction model, ∘ CONTACT ; (b) relative difference.

3.2 Smooth surfaces

The simulation presented in section 3.1 is now repeated with the Green's functions obtained from the receptances in Figure 2.

The time series of the contact forces is presented in Figure 6, where the first 72 ms correspond to the period of preload application. After some initial oscillations the contact forces go towards a steady-state solution. Due to the influence of the structural dynamics of wheel and track, this steady-state solution differs slightly from the quasi-static case in section 3.1. The vertical contact force increases to $F_3 = 65.8\,\mathrm{kN}$, while the lateral force decreases (in absolute value) to $F_2 = -7.4\,\mathrm{kN}$.

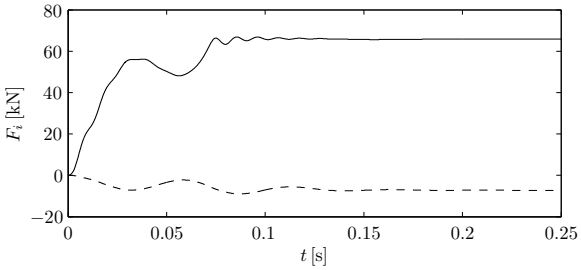

FIG. 6: Dynamic contact forces, smooth surfaces, $\eta = 10^{-3}$. —— vertical, − − −, lateral.

In comparison to the quasi-static case, one contact element changed from the slip zone to the stick zone (Figure 7) and the distribution of the lateral tangential stress varies slightly (Figure 8).

The higher the imposed lateral creepage, the bigger is the influence of the structural dynamics of wheel and track. In the case $\eta = 10^{-2}$, where the complete contact area is in slip, the steady-state vertical contact force is $F_3 = 67.2\,\mathrm{kN}$.

3.3 Rough surfaces

In this section, one example is shown where the interaction model is applied for rough surfaces. The rough-

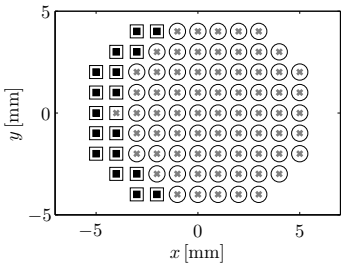

FIG. 7: Division of the contact area : smooth surfaces, $\eta = 10^{-3}$. Stick zone : ∘ (CONTACT), x (interaction model) ; Slip zone : □ (CONTACT), □, filled (interaction model).

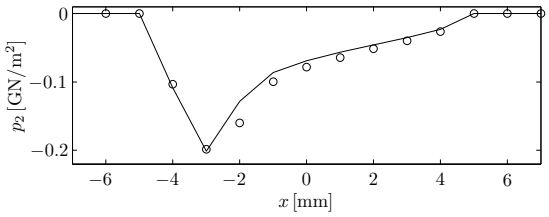

FIG. 8: Lateral tangential stress on line $y = 0$: smooth surfaces, $\eta = 10^{-3}$. —— interaction model, ∘ CONTACT.

ness used is a wheel roughness data set measured on a wheel with sinter block brakes in 25 parallel lines with a spacing of 2 mm across the width of the running surface [13]. The roughness level is low over the whole frequency range of interest. More information about the roughness data set can be found in [14], where it is referred to as 'wheel 1 with sinter block brakes'.

Figure 9 shows the time series of the dynamic contact forces. For two instants in time, t_1 and t_2, the corresponding divisions of the contact area into stick and slip zones and the lateral tangential stress distribution at $y = 0$ are presented in Figures 10 and 11, respectively. The comparison to the results from CONTACT reveals that the shape of the contact area and the stick and slip zones can differ considerably from the quasi-static case. The same is true for the tangential stress distribution.

4 Conclusions

A numerical model has been presented, which simulates high-frequency wheel/rail interaction including tangential friction in the time-domain. As wheel and track are represented by pre-calculated impulse response functions, the model is characterised by high computational efficiency. This makes it possible to include a non-steady state contact model that is solved at each time step in the interaction model. The comparison of the interaction model with Kalker's rolling contact model CONTACT for a quasi-static case shows that the implementation of the contact model is correct. Results from the interaction model for dynamic cases with smooth and rough wheel and rail surfaces differ from CONTACT. This is explained by the fact that the interaction model includes the structural dynamics of wheel and rail and the effect of surface roughness.

Future work will include the implementation of a

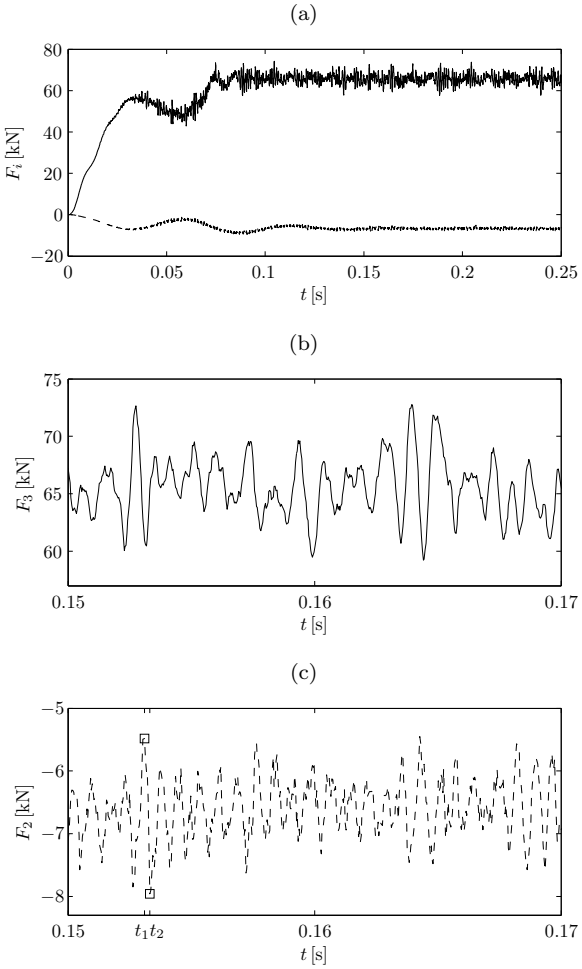

FIG. 9: Dynamic contact forces : rough wheel, $\eta = 10^{-3}$: —— vertical, − − − lateral ; (a) time series from $t = 0$; (b) zoom F_3 ; (c) zoom F_2.

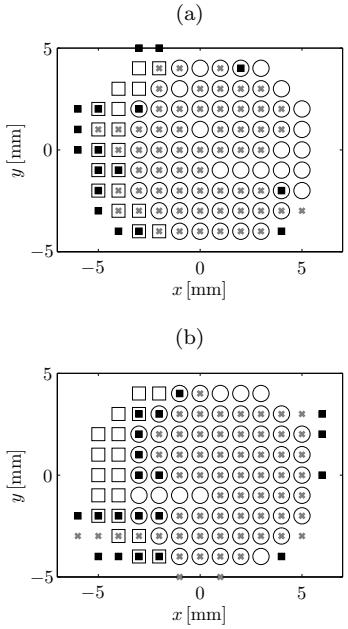

FIG. 10: Division of the contact area : rough wheel, $\eta = 10^{-3}$. Stick zone : ∘ (CONTACT), x (interaction model) ; Slip zone : □ (CONTACT), □, filled (interaction model) ; (a) at t_1 in Figure 9(c) ; (b) at t_2 in Figure 9(c).

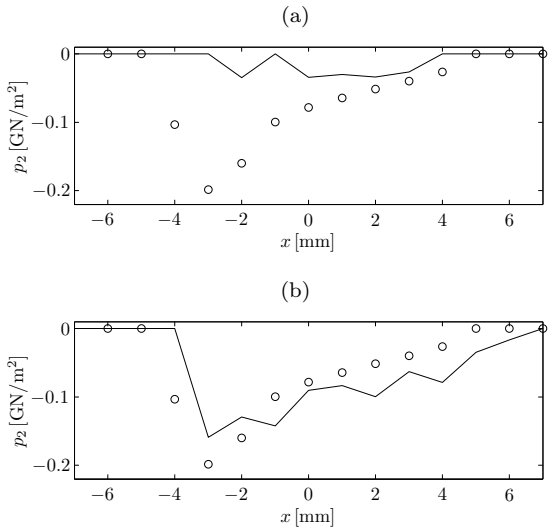

FIG. 11: Lateral tangential stress on line $y = 0$: rough wheel, $\eta = 10^{-3}$; ——— interaction model, ∘ CONTACT ; (a) at t_1 in Figure 9(c) ; (b) at t_2 in Figure 9(c).

velocity-dependent friction coefficient, which implies an extension of the contact model. Furthermore, the validation of the interaction model for dynamic cases is an important aspect of future work.

Acknowledgements

The authors are grateful for the support by Prof. David Thompson (ISVR, University of Southampton) who supplied us with the wheel model used in this paper. Furthermore, we would like to thank Dr. Briony Croft (former PhD student at ISVR) for her help with the implementation of the wheel model. Finally, the access to the Wave Guide Finite Element toolbox WANDS (developed by the Dynamics Group at ISVR), which has made the modelling of the track to an easy and efficient task, is greatly acknowledged.

Références

[1] Thompson D., "Railway Noise and Vibration : Mechanisms, Modelling and Means of Control", Elsevier, Oxford, UK (2009)

[2] Rudd M.J., "Wheel/rail noise - Part II : Wheel squeal", *J. Sound Vib.* 46 (3), 381-394 (1976)

[3] Heckl Maria A., Abrahams I.D. "Curve squeal of train wheels, Part 1 : Mathematical model for its generation ", *J. Sound Vib.* 229 (3), 669-693 (2000)

[4] de Beer F.G., Janssens M.H.A., "Squeal noise of rail-bound vehicles influenced by lateral contact position", *J. Sound Vib.* 267, 497-507 (2003)

[5] Chiello O., Ayasse J.-B., Vincent N., Koch J.-R. "Curve squeal of urban rolling stock - Part 3 : Theoretical model", *J. Sound Vib.* 293, 710-727 (2006)

[6] Huang Z.Y., Thompson, D.J., Jones C.J.C. "Squeal Prediction for a Bogied Vehicle in a Curve", in Schulte-Werning B. et al. (Eds.) : *Noise and Vibration Mitigation*, NNFM 99, 313-319 (2008)

[7] Wullens F., Kropp W. "A three dimensional contact model for tyre/road interaction in rolling conditions", *Acta Acust. United Ac.* 90 (4), 702-711 (2004)

[8] Pieringer A., Kropp W., Nielsen J.C.O. "A Time Domain Model for Wheel/Rail Interaction Aiming to Include Non-linear Contact Stiffness and Tangential Friction", in Schulte-Werning B. et al. (Eds.) : *Noise and Vibration Mitigation*, NNFM 99, 285-291 (2008)

[9] Nilsson C.-M., Jones C.J.C., Thompson D.J., Ryue, J. "A waveguide finite element and boundary element approach to calculating the sound radiated by railway and tram rails", *J. Sound Vib.* 321, 813-836 (2009)

[10] Nordborg A., "Wheel/rail noise generation due to nonlinear effects and parametric excitation", *J. Acoust. Soc. Am.* 111 (4), 1772-1781 (2002)

[11] Kalker J.J., "Three-Dimensional Elastic Bodies in Rolling Contact", Kluwer Academics Publishers, Dordrecht, The Netherlands (1990)

[12] Vollebregt E.A.H., "User's Guide for CONTACT, J.J. Kalker's variational contact model", Technical Report, TR09_03, version 0.9, VORtech Computing, Delft, The Netherlands (2009)

[13] Thompson D.J., Remington P.J., "The effects of transverse profile on the excitation of wheel/rail noise", *J. Sound Vib.* 231 (3), 537-548 (2000)

[14] Pieringer A., Kropp W., Thompson D., "Investigation of the dynamic contact filter effect in vertical wheel/rail interaction using a 2D and a 3D non-Hertzian contact model", *Proceedings of the 8th International Conference on Contact Mechanics and Wear of Rail/Wheel Systems*, vol. 1, 105-113, Firenze, Italy (2009).